Progress In Electromagnetics Research C, Vol. 65, 163–173, 2016

Dual Band-Notched WIMAX/WLAN of a Compact Ultrawideband Antenna with Spectral and Time Domains Analysis for Breast Cancer Detection

Abdelmoumen Kaabal[1, *], Mustapha El halaoui[1], Saida Ahyoud[2], and Adel Asselman[1]

Abstract—A compact Ultra Wideband (UWB) antenna with Worldwide Interoperability for Microwave Access (WiMAX) and Wireless Local Area Network (WLAN) with dual-band notched characteristics is presented in this article. The antenna design parameters have been optimized by the High Frequency Structural Simulator (HFSS) and CST Microwave Studio to be in contact with biological breast tissues over 3–13 GHz frequency range with dual band-notched characteristics. The proposed antenna is a polygon printed on a low dielectric FR4 substrate fed by a 50-Ω feed line and a partial ground plane in other side. The results exhibit that the proposed antenna shows a wide bandwidth covering from 3 GHz to at least 13 GHz with VSWR < 2 and observing band elimination of WiMAX and WLAN bands. The proposed UWB antenna has omnidirectional radiation patterns with a gain variation of 0.5 dBi to 5.2 dBi and low distortion group delay less than 1 ns over the operating frequency range. The simulation and measurement results show a good agreement. And good ultra-wideband linear transmission performance has been achieved in time domain with a compact dimension of $28 \times 20\,\text{mm}^2$.

1. INTRODUCTION

Ultra-wideband (UWB) communication systems have become a most promising candidate for short-range high-speed indoor data communications since the US-FCC released the bandwidth from 3.1 GHz to 10.6 GHz in 2002 [1, 2]. Higher data rates, saturation of the frequency spectrum and low power consumption are some of the reasons that ultra-wideband has received increased interest over the past years [3–8]. UWB systems, in comparison with conventional or narrowband systems, use a large bandwidth to transmit the information. The power used over the whole band is much lower than the power used by narrowband systems. Furthermore, the existence of other wireless narrow bands requires rejection of certain frequencies within the UWB band [9–11]. Due to the frequency characteristic variation of the ultra-wideband technology, the antennas should be analyzed in the time domain as well [12]. One important characteristic of ultra-wideband technology is the transmission of very short pulses in time having a very broad frequency spectrum [13]. The frequency characteristics of narrowband antennas are constant over their operational bandwidth, hence they can be fully characterized in the frequency domain. Standard parameters such as return loss, gain and radiation efficiency have been defined for narrowband antennas. However, UWB antennas are meant to transmit not continuous pulsed signals. Most simulation tools present the results in the frequency domain, and many limitations were encountered, even if they use a time domain technique to compute the fields, showing that the available techniques do not analyze the most important parameters of UWB antenna simultaneously [14]. So analyzing them only in the frequency domain is not enough to fully evaluate their performance, as pulse

Received 15 April 2016, Accepted 27 May 2016, Scheduled 5 July 2016

* Corresponding author: Abdelmoumen Kaabal (kaabal.abdelmoumen@gmail.com).

[1] Optics and Photonics Team, Faculty of Sciences, Abdelmalek Essaadi University, P. O. Box: 2121, Tetouan, Morocco. [2] Information Technology and Systems Modeling Team, Faculty of Sciences, Abdelmalek Essaadi University, P. O. Box: 2121, Tetouan, Morocco.

distortion is an important parameter that should be controlled. When characterizing the performance of UWB antennas, such as fidelity, transfer function (impulse response in the time domain), wave response and group delay will be necessary [15]. This is therefore a strong motivation to analyze the antenna behavior when transmitting pulses signals. An antenna should be able not only to radiate over the entire desired frequency band, but also to radiate a pulse without any distortion, or as small distortion as possible [16, 17]. The objective of this article is to implement a UWB antenna with WiMaX/WLAN dual band-notched characteristics in the time domain analysis. Different characterization methods available today were studied in order to identify the most important parameters describing UWB antennas. Furthermore, measurements of the available methods are not always possible to realize using the available equipment, which is typically in frequency domain for antenna analysis. The UWB antenna will be in contact with biological breast tissue to expel the impact of the proximity of the biological tissue for detection of tumors within the breast of women [18–20].

2. THE PROPOSED ANTENNA CONFIGURATION

2.1. Antenna Design Geometry

The design geometry process of the proposed antenna is shown in Fig. 1. The antenna optimized to operate at UWB range frequencies with a width band of 3 GHz to at least 13 GHz as well as voltage standing wave ratio less than two (VSWR < 2) and to radiate nearly omnidirectionally. The proposed antenna has been designed by selecting a polygon patch of five edges and printed on the side of an FR4 substrate whose surface is 28 mm $\times$ 20 mm, with thickness of 1.6 mm, permittivity of 4.4, loss tangent of 0.02 and copper foil thickness of 35 µm. On a partial ground plane to support UWB range frequencies in the opposite side of the substrate, a defected slot is added in the middle of the ground plane to increase the reflected power [10]. The antenna is excited using a 50-Ω feed line and optimized using HFSS and CST Microwave Studio. The detailed geometry and parameters are shown in Fig. 1 and Table 1.

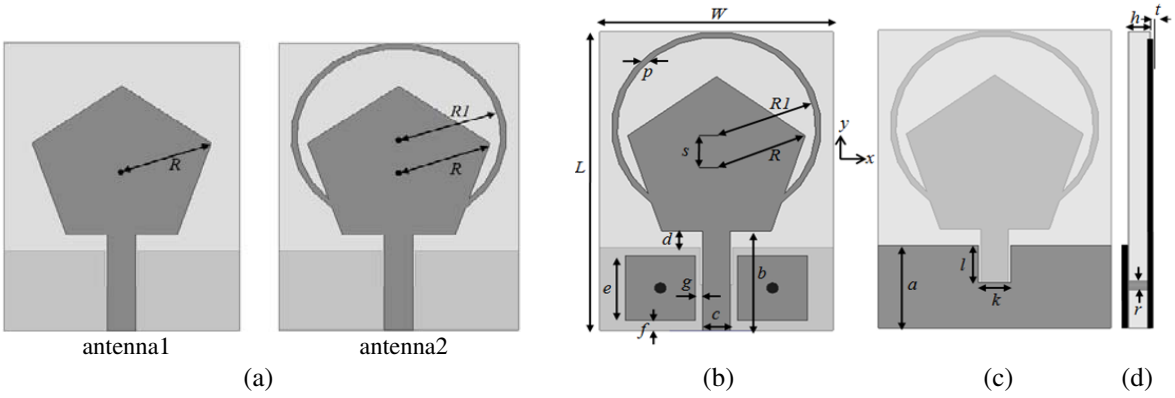

Figure 1. Geometry of proposed UWB antenna. (a) Top view without EBG, (b) top view of the proposed antenna, (c) bottom view and (d) side view.

Table 1. Optimal design parameters of UWB antenna.

Parameter	value (mm)	Parameter	value (mm)	Parameter	value (mm)
L	28	s	3.2	t	0.035
W	20	$R1$	8.5	r	1
a	7.8	R	8	p	0.5
l	3.5	e	3.1	b	9.3
k	2.8	f	0.7	c	2.4
h	1.6	g	0.4	d	1.5

2.2. Antenna Results and Discussion

The antenna results and discussion are divided into two parts which consist of parametric study and experimental results with a discussion. The parametric study including the simulated results of return loss with different effects of design parameters, such as gain, radiation efficiency and radiation patterns of the proposed antenna, are presented in Part I. In Part II, measurement results of the fabricated antenna are presented and discussed.

2.2.1. Parametric Study

The antenna design is optimized with the study of some parameters' effect. Fig. 2 shows the return loss against frequency of antenna1 according to the radius (R) of the polygon. It is observed that for values of R between 6.5 mm and 9 mm, the reflected power increases over the operation frequency range when R decreases.

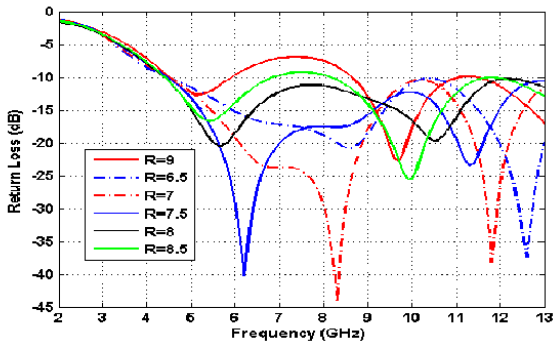

Figure 2. Effect of radius R for antenna1.

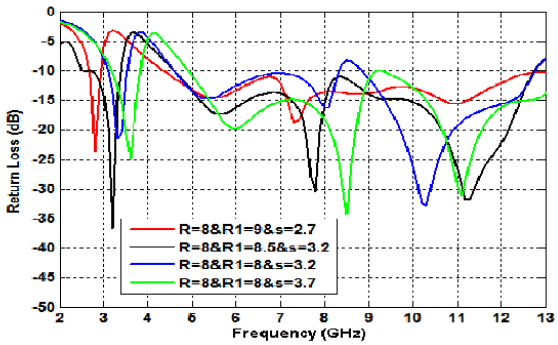

Figure 3. Effect of radius $R1$ for antenna2.

For the notched UWB antenna, the antenna accompanies firstly with a ring slot of radius $R1$ and surrounds the polygon radiator element to reject WiMAX band from 3.2 GHz to 4.2 GHz. The effect of radius $R1$ and s parameters for $R = 8$ mm are shown in Fig. 3. It is found that high value of $R1$ forces the antenna to operate at lower frequencies less than 3 GHz, whereas the notched band tended to move toward lower frequencies. On the other hand, for the same value of $R1$, high value of s parameter moves the notched band towards higher frequencies. The s parameter is changed to avoid the intersection between the ring slot and polygon radiator element, or to avoid to be outside of the antenna dimension. It can be noted that the position of the notched band is changed when this antenna is associated with EBG structures. To obtain a dual notched band antenna, a pair of EBG structures is added to antenna2. The EBG parameters are optimized by calculating the reflection phase response

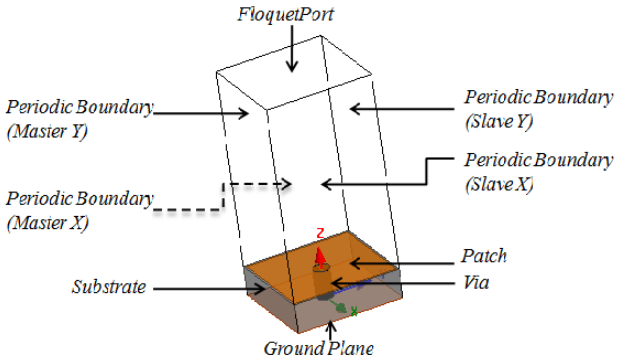

Figure 4. The unit cell setup of reflection phase model in HFSS with the boundary conditions.

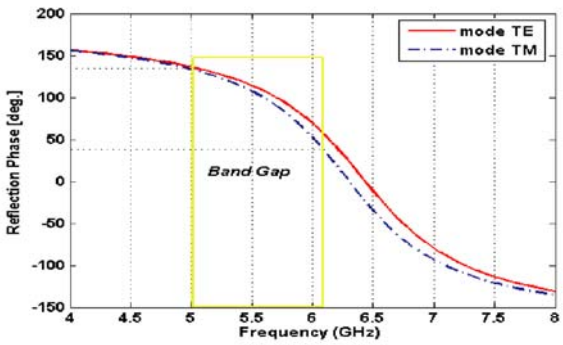

Figure 5. Reflection phase response of EBG structures.

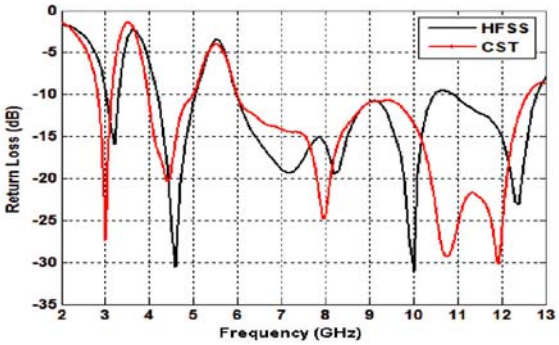

Figure 6. Return loss of the proposed UWB antenna.

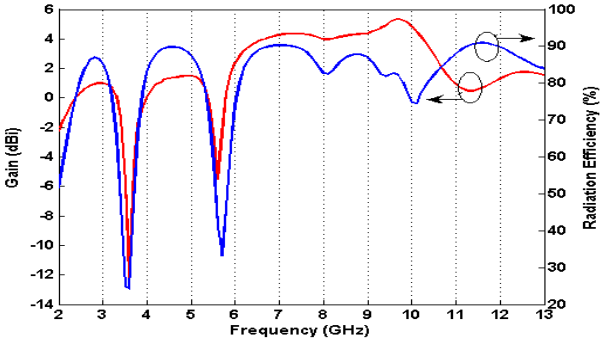

Figure 7. Simulated peak gain and radiation efficiency of the proposed UWB antenna.

using ansoft HFSS, and the optimal values are shown in Table 1. The unit cell of the structure under investigation has to be drawn with periodic boundary conditions applied in the appropriate directions (Fig. 4). The reflection phase response (Fig. 5) of the EBG structure shows a stop band obtained in the frequency range 5 GHz to 6 GHz with a reflection phase in the range of $+90° \pm 45°$ [21]. Finally, Fig. 6 shows the final simulation results from CST Microwave Studio and HFSS.

Figure 7 gives the peak gain and radiation efficiency of the proposed UWB antenna. It can be seen that the peak gain varies between 0.5 dBi and 5.2 dBi within the operating frequency band of the antenna, while the radiation efficiency reaches values greater than 80%. Both the peak gain and radiation efficiency have a significant drop in the rejected band where the antenna incorporates the EBG structure and ring slot. The radiation patterns of the proposed antenna at 3 GHz, 4.5 GHz, 5.5 GHz, 7 GHz and 10 GHz for the elevation plane pattern and azimuth plane pattern are illustrated in Fig. 8. It can be seen that the antenna almost achieves omnidirectional radiation pattern over the whole UWB frequency range.

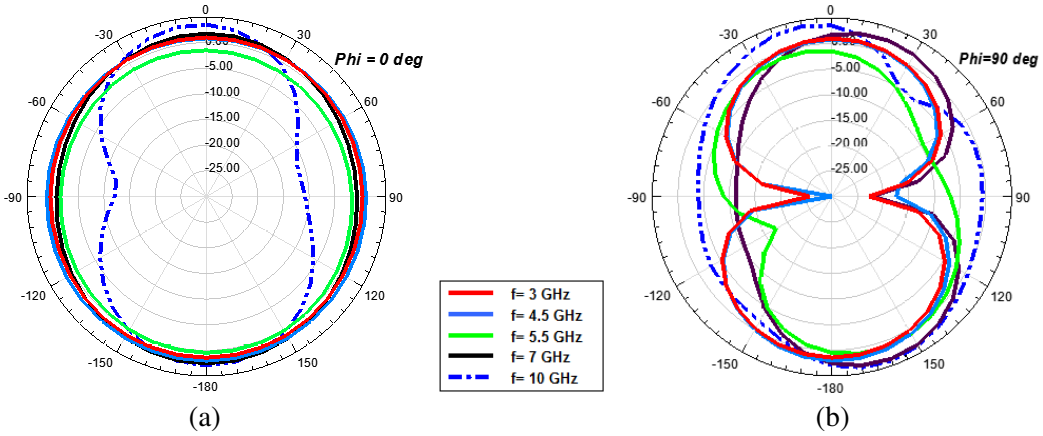

Figure 8. Simulated radiation pattern, (a) elevation plane pattern, (b) azimuth plane pattern.

2.2.2. Measurement Results and Discussion

Figure 9 shows a prototype of the proposed antenna. The antenna has been fabricated using conventional printed circuit board (PCB) design techniques. Fig. 10 shows the simulated and measured results of the proposed antenna integrated with EBG structure and ring slot to obtain a dual band-notched antenna for WiMAX (3.2 GHz to 4.2 GHz) and WLAN (5 GHz to 6 GHz). There is a good agreement between the measured and simulated results. The results have validated that the proposed antenna design can eliminate the interference among UWB application for breast cancer detection and WiMAX/WLAN systems.

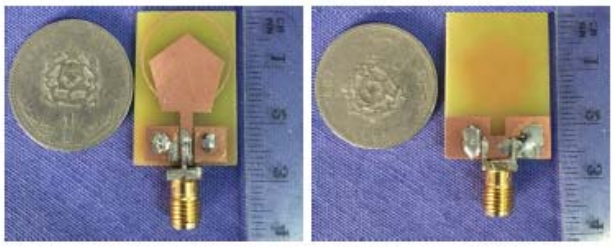

Figure 9. Prototype of the proposed antenna.

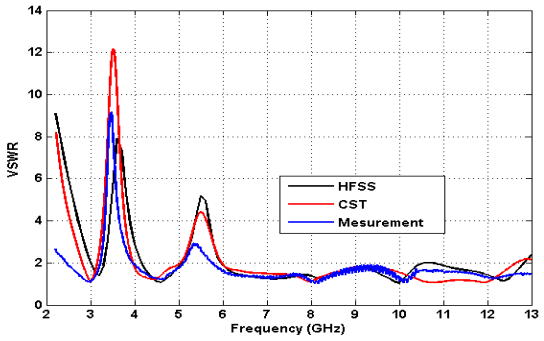

Figure 10. Simulated reflection coefficients with variation of the width of the two elements.

3. CHARACTERIZATION OF PROPOSED UWB ANTENNA PERFORMANCE IN TIME DOMAIN

3.1. Waveform Response

In CST Microwave Studio, the UWB antenna is inspired by the transient Gaussian pulse, and the frequency spectrum covers the entire UWB frequencies [22, 23]. The input signal and the magnitude power spectrum at the transmitting antenna terminal is illustrated in Fig. 11.

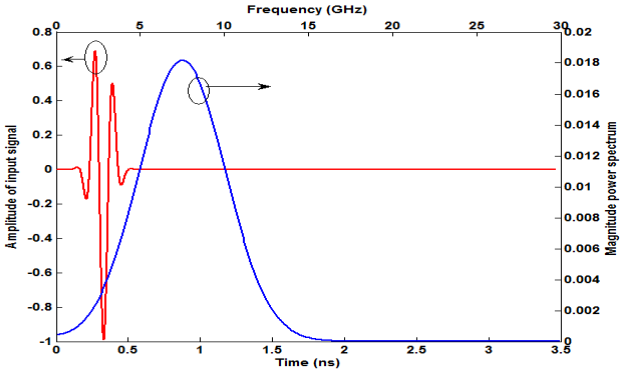

Figure 11. Normalized excitation signal and its spectral density.

The waveform response and frequency spectra of the reflected and transmitted signals of the antenna are plotted as shown in Fig. 12. As shown in Fig. 12(b), the rejected bands of frequency spectra are observed at corresponding notched band. The waveforms are obtained by placing a pair of identical antennas face-to-face with a distance of 150 mm to determine the waveform distortion and time delay. To appraise time-domain performances of the antenna more objectively, group delay of the transmitted signal and correlation coefficient are calculated in the following section.

3.2. Group Delay

The essential factor of a high-quality UWB antenna is minimal pulse distortion. To avoid waveform distortion, a linear phase response of antenna (constant group delay) is desired to characterize its time-domain property. Group delay is a measure of the transit time of a signal through a device versus frequency (Eq. (1)).

$$\text{group delay} = -\frac{\Delta\varphi}{\Delta\omega} \tag{1}$$

where φ is the phase of transmission coefficient S_{12} and $\omega = 2\pi f$.

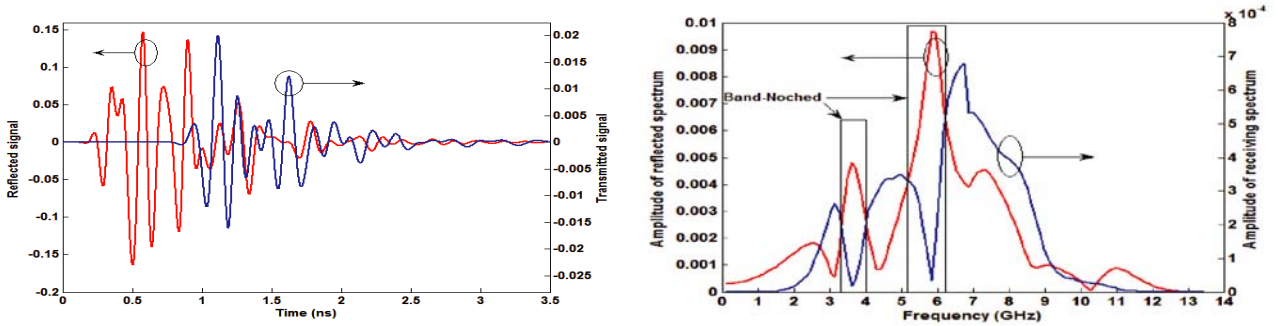

(a) (b)

Figure 12. Waveform responses of the antenna (a) in the time domain and (b) in the frequency domain.

The results are exhibited in Fig. 13. The variation in group delay is caused by signal distortion, whereas a constant group delay implies perfect signal transmission.

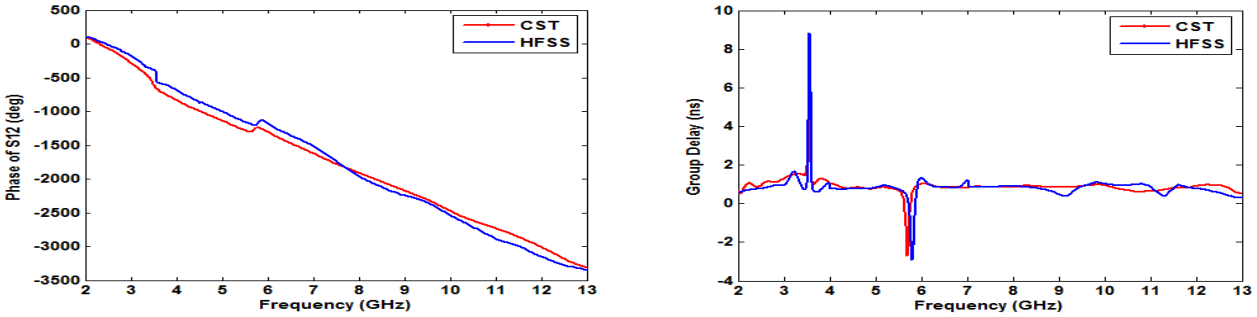

(a) (b)

Figure 13. (a) Phase of S_{12}, (b) group delay responses.

In this figure, a sharp variation of group delay with a narrow width in the vicinity of the dual band-notched antenna is observed, indicating the effect of EBG structure and ring slot, which can break down the constant group delay requirement. However, the variation of group delay is very small, even negligible, less than 1 ns within the operating frequency range, which indicates good linear phase responses and assures that the energy is concentrated on the pass band of the proposed antenna.

3.3. Correlation Coefficient

The correlation coefficient is a measure of similarity of two waveforms as a function of a time-lag applied to one of them. It compares the incident signal $S_1(t)$ and receiving signal $S_2(t)$ (the electric field intensity signal or the receiving antenna signal) at far-field region. The incident signal, $S_1(t)$, of UWB antenna undergoes a distortion induced by the antenna, and this signal distortion can be quantified first by finding the correlation between the incident signal and receiving one. The correlation function is:

$$H(\tau) = \int_{-\infty}^{+\infty} s_1(t)s_2(t-\tau)dt \tag{2}$$

The received signal $S_2(t)$ can be obtained by virtual probes at the far-field placing in 150 mm distance from transmitting antenna, and the correlation coefficient can be found by determining the maximum value of the weighted correlation between $S_1(t)$ and $S_2(t)$ [24, 25]:

$$\rho = \frac{\displaystyle\int_{-\infty}^{+\infty} s_1(t)s_2(t-\tau)dt}{\sqrt{\left(\displaystyle\int_{-\infty}^{+\infty} s_1^2(t)dt\right)}\sqrt{\left(\displaystyle\int_{-\infty}^{+\infty} s_2^2(t)dt\right)}} \tag{3}$$

where τ is the time delay of the signal and $0 \leq \rho \leq 1$. Ideally, the correlation coefficient should be as close to 1 as possible, indicating low distortion created by the antenna and a perfect signal transmission. A value of 0 means the received pulse is completely different from the one at the input antenna port. The transmitted signal is totally distorted, and the received pulse amplitude is nil. The time domain analysis is a measurement technique where the electric probe is placed at different positions to investigate the transmitted and received pulse signals. Virtual probes measuring the electric field placed at a distance of 150 mm from the input signal at the transmitting antenna terminal and the far-field receiving signal for various angles are shown in Fig. 14.

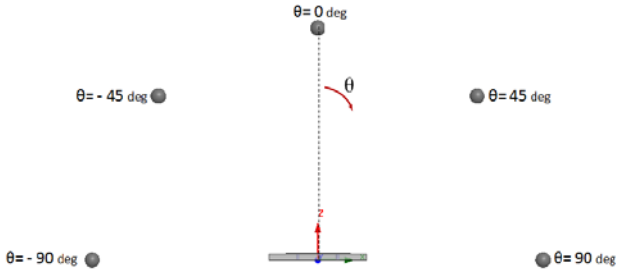

Figure 14. Location of the probes around the antenna in the vertical $y = 0$ plane.

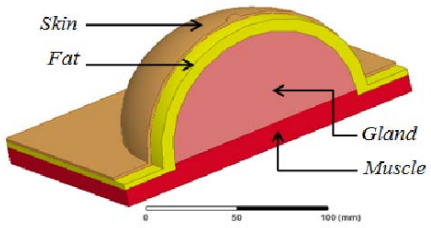

Figure 15. Multi-layer inhomogeneous model of the breast designing in HFSS.

Table 2. The correlation coefficient values for deferent values.

	Position of Electric field intensity signal at deferent position		
	$\theta = 0$ deg	$\theta = 45$ deg	$\theta = 90$ deg
Correlation coefficient	0.941106	0.901518	0.785813

The values of the correlation coefficient derived from electric field intensity signal for various angles are calculated using Eq. (3) and presented in Table 2.

It is found from the table that the values of the correlation coefficient are larger than 0.7. Nevertheless, the correlation coefficient is lower at $\theta = 90$ deg than at $\theta = 0$ deg by almost 16.5%. The low correlation coefficient coincides with the low gain points in its gain pattern.

4. APPLICATION OF THE ANTENNA TO DETECT BREAST CANCER

4.1. Breast Model

The compact UWB antenna is designed to be in contact with biological breast tissues over 3–13 GHz frequency range with dual notched-band. After establishing the transmitted signal, this signal was transmitted through an antenna and into a sample of a biological breast tissue [26]. A breast model should be designed with an inhomogeneous medium to capture all phenomena during the design process,

Table 3. Dielectric properties for the different tissue types found in the breast.

Tissue type	Dielectric constant (mm)	Conductivity (S/m)	Masse density (kg/m^3) (mm)
Skin	36	4	1010
Fat	9	0.4	928
Gland	16	1	1035
Muscle	50	7	1040
Tumor	50	7	1040

and the multilayer model is used to represent the inhomogeneous medium of the breast tissues including skin, fat, gland and muscle as shown in Fig. 15. The dielectric properties for the different tissue types found in the breast are given in Table 3 [27–30]. The dielectric parameters for the tumor are assumed to be the same as those of muscle.

4.2. Waveform Response and Detection of the Breast Cancer

The proposed antenna is designed to operate in contact with stacked layers of biological tissue in a detection system. Using UWB pulses, the scattering parameters of antenna made it easy to observe differences between the transmitted signal through the breast tissue and the tumor cells. The electric field waveforms as a function of the observation angle in the vertical direction at a constant distance of 150 mm between the antenna and virtual probes at the far-field in vacuum and in the presence of a biological breast tissue with and without tumor were obtained and presented in Fig. 16. From this figure, it is observed that the amplitude of the transmitted signal is very large in the vacuum because of the homogeneity of the medium. Otherwise, the existence of the biological tissue produces multiple reflections on the surfaces of each layer constituting the breast, and consequently, there are energy losses during transmission, so the transmitted signal amplitude decreases. Furthermore, the existence of the tumor in the gland decreased energy which transmitted in a very strong manner due to the dielectric properties varied with respect to those of the gland. On the other hand, face-to-face position (Fig.16(a)) is the best position of the breast cancer detection because the energy transmitted in the existence of tumor is very low in this direction due to strong reflection across the tumor. For other positions, the signal undergoes a partial reflection across the tumor, which leads to increasing the transmitted signal amplitude and consequently, the bad position when $\theta = 90$ deg (Fig. 16(c)). Finally, due to the variance of the dielectric properties between the breast tissue and the tumor cells, the breast cancer detection becomes possible. We cannot avoid the power reflections (between tissues) caused by inhomogeneities

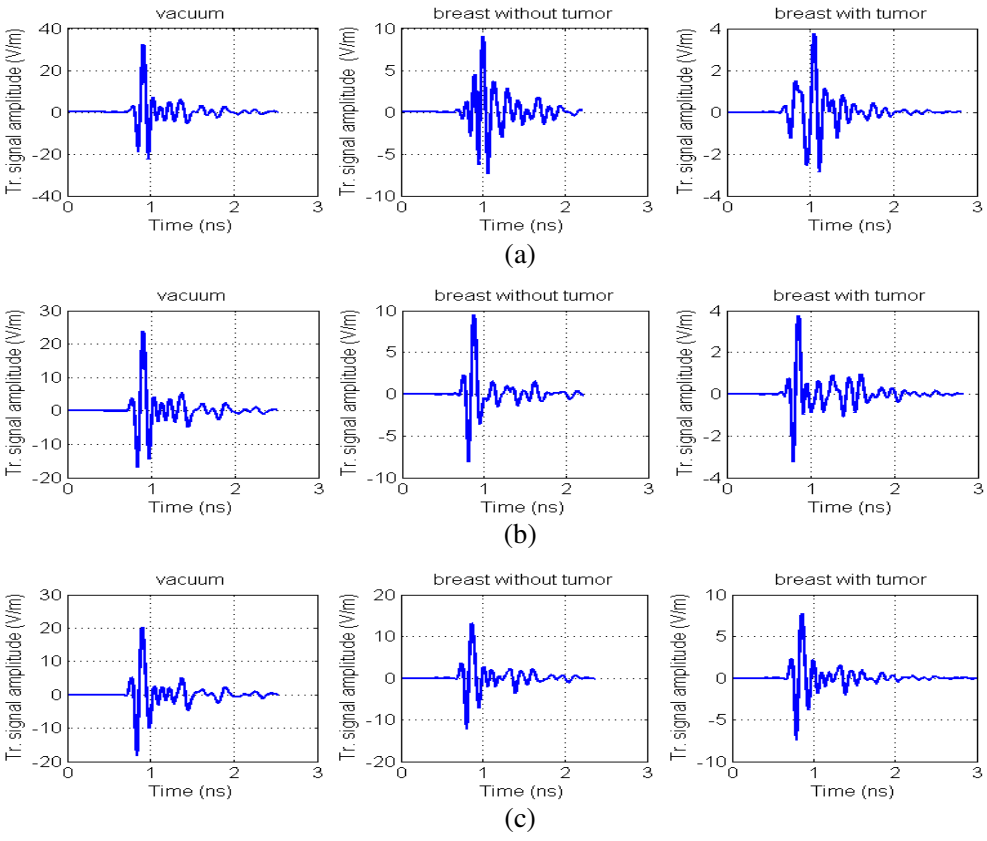

Figure 16. Wave response: (a) $\theta = 0$ deg, (b) $\theta = 45$ deg and (c) $\theta = 90$ deg.

in the breast media, and the antenna must provide as much energy as possible in order to receive transmitted signals with reasonable amplitudes from breast tissues. Therefore, for women with larger breast sizes, the detection of the pulse will be difficult considering maximum allowable power.

4.3. Propagation of EM Wave in Breast Tissue

Figure 17 visualizes the propagation of electromagnetic waves in the dielectric properties of breast tissue.

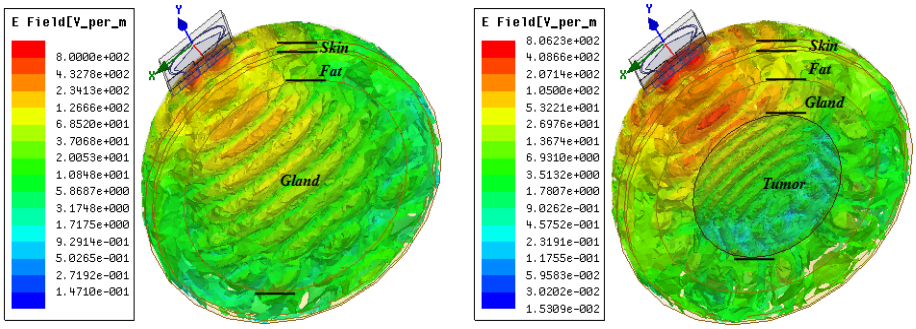

(a) 6 GHz

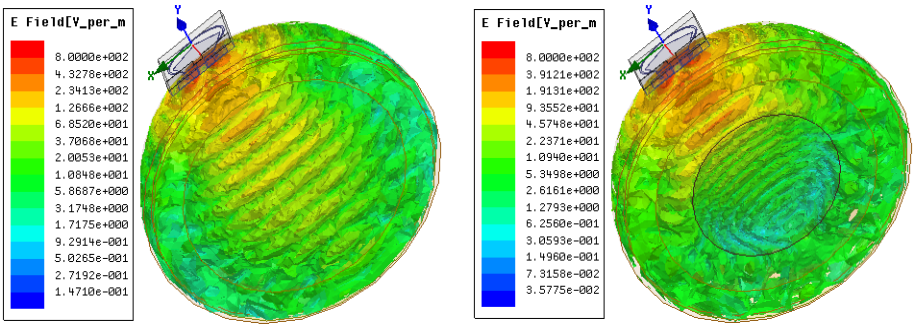

(b) 7 GHz

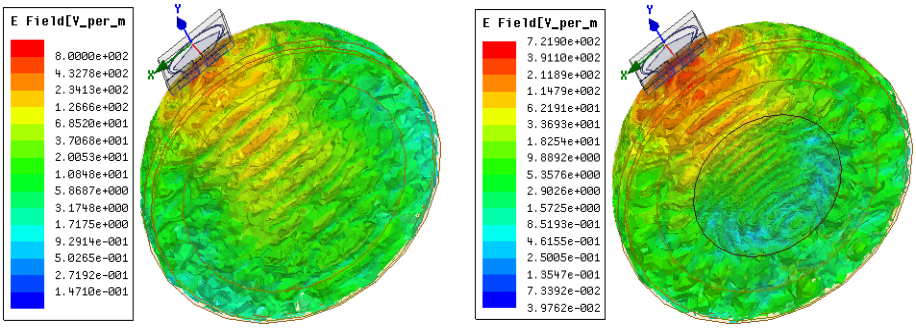

(c) 8 GHz

Figure 17. Propagation of F-field intensity in breast tissue. (a) 6 GHz, (b) 7 GHz, (c) 8 GHz.

It is observed from this figure that the E-field is more intense in the vicinity of the antenna, which shows significant absorption by the breast tissue. Otherwise, during propagation, the amplitude of the E-field is attenuated due to the multiple reflections across various mediums constituting the breast. However, the existence of a tumor prevents the electromagnetic waves to propagate and behaves as an electric wall, which means the decrease in amplitude of the transmitted signal through the breast tissue presented in Fig. 16.

5. CONCLUSION

In this paper, we proposed a UWB antenna for breast cancer detection. The optimization of the proposed antenna has been obtained, which covers an impedance bandwidth of 3 GHz to 13 GHz. Besides, a simulation of radiation patterns, antenna gain, group delay and correlation coefficient were shown. Furthermore, to improve the antenna's performance, the ring slot and EBG structure were added to the proposed antenna, in turn providing a stop band approximately 3.2 GHz to 4.2 GHz and 5 GHz to 6 GHz, respectively, which is capable of reducing potential interference between UWB and WIMAX/WLAN communication systems. The EBG structure and ring slot had a little effect on the antenna's performance and had a high distortion of transmitted signal on the notched WIMAX and WLAN bands. The group delay variation was less than 1 ns, which indicated that the antenna presented had a good pulse preserving capability. A comparison between simulation and measurement showed an excellent agreement among the results and validated the design process presented in this paper. A negligible dispersion over the operating frequency range and a small size $28 \times 20\,\text{mm}^2$ of antenna reduced the error associated with antenna's position, and thus, improved the accuracy of the system, which made it suitable for UWB breast cancer applications.

ACKNOWLEDGMENT

The authors would like to express their deepest gratitude to Naima A. Touhami from Electronics Instrumentation and microwave Laboratory, Faculty of Sciences, Abdelmalek Essaadi University, for the measurement and the technical support.

REFERENCES

1. "FCC 1st report and order on ultra-wideband technology," Feb. 2002.
2. Low, Z. N., J. H. Cheong, and C. L. Law, "Low-cost PCB antenna for UWB applications," *IEEE Antennas and Wireless Propagation Letters*, 237–239, 2005.
3. Lim, K.-S., M. Nagalingam, and C.-P. Tan, "Design and construction of microstrip UWB antenna with time domain analysis," *Progress In Electromagnetics Research M*, Vol. 3, 153–164, 2008.
4. Lee, J. N., "Design of an ultra-wideband antenna using a ring resonator with a notch function," *ETRI Journal*, Vol. 35, No. 6, 1075–1083, Dec. 2013.
5. Trinh-Van, S. and C. Dao-Ngoc, "Dual band-notched UWB antenna based on electromagnetic band gap structures," *REV Journal on Electronics and Communications*, Vol. 1, No. 2, Jun. 2011.
6. Pandey, G. K., H. S. Singh, P. K. Bharti, and M. K. Meshram, "Design of WLAN band notched UWB monopole antenna with stepped geometry using modified EBG structure," *Progress In Electromagnetics Research B*, Vol. 50, 201–217, 2013.
7. Peng, L. and C.-L. Ruan, "Design and time-domain analysis of compact multi-band-notched UWB antennas with EBG structures," *Progress In Electromagnetics Research B*, Vol. 47, 339–357, 2013.
8. Manurkar, R. P. and V. G. Kasabegoudar, "Four ports wideband pattern diversity MIMO antenna," *Global Journal of Researches in Engineering*, Vol. 15, No. 3, 2015.
9. Akhoondzadeh-Asl, L., M. Fardis, A. Abolghasemi, and G. R. Dadashzadeh, "Frequency and time domain characteristic of a novel notch frequency UWB antenna," *Progress In Electromagnetics Research*, Vol. 80, 337–348, 2008.
10. Kaabal, A., S. Ahyoud, and A. Asselman, "A new design of star antenna for ultra wide band applications with WLAN-band-notched using EBG structures," *International Journal of Microwave and Optical Technology*, Vol. 9, No. 5, 544–548, Sep. 2014.
11. Islam, M. M., M. R. I. Faruque, and M. T. Islam, "A compact 5.5 GHz band-rejected UWB antenna using complementary split ring resonators," *The Scientific World Journal*, Vol. 2014, 1–8, 2014.
12. Quintero, G., J.-F. Zurcher, and A. K. Skrivervik, "System fidelity factor: A new method for comparing UWB antennas," *IEEE Transactions on Antennas and Propagation*, Vol. 59, No. 7, 2502–2512, Jul. 2011.

13. Kim, S. H., Z.-J. Jin, Y.-B. Chae, and T.-Y. Yun, "Small internal antenna using multiband, wideband, and high-isolation MIMO techniques," *ETRI Journal*, Vol. 35, No. 1, 51–57, Feb. 2013.
14. Quintero, G. and D. de Leon, "Analysis and design of ultra-wideband antennas in the spectral and temporal domains," *Ecole Polytechnique Fédérale de Lausanne*, Lausanne, 2010.
15. Quintero, G., J. F. Zurcher, and A. K. Skrivervik, "System fidelity factor: A new method for comparing UWB antennas," *IEEE Transactions on Antennas and Propagation*, Vol. 59, No. 7, 2502–2512, Jul. 2011.
16. Wiesbeck, W., G. Adamiuk, and C. Sturm, "Basic properties and design principles of UWB antennas," *Proceedings of the IEEE*, Vol. 97, No. 2, 372–385, Feb. 2009.
17. Augustin, G., B. P. Chacko, and T. A. Denidni, "Dual port ultra wideband antennas for cognitive radio and diversity applications," *Advancement in Microstrip Antennas with Recent Applications*, A. Kishk, Ed., InTech, 2013.
18. Sugitani, T., S. Kubota, A. Toya, X. Xiao, and T. Kikkawa, "A compact 4×4 planar UWB antenna array for 3-D breast cancer detection," *IEEE Antennas and Wireless Propagation Letters*, Vol. 12, 733–736, 2013.
19. Zwick, T., L. Zwirello, M. Jalilvand, and X. Li, "Ultra wideband compact near-field imaging system for breast cancer detection," *IET Microwaves, Antennas and Propagation*, Vol. 9, No. 10, 1009–1014, Jul. 2015.
20. Chahat, N., M. Zhadobov, R. Sauleau, and K. Ito, "A compact UWB antenna for on-body applications," *IEEE Transactions on Antennas and Propagation*, Vol. 59, No. 4, 1123–1131, 2011.
21. Yang, F. and Y. Rahmat-Samii, "Reflection phase characterizations of the EBG ground plane for low profile wire antenna applications," *IEEE Transactions on Antennas and Propagation*, Vol. 51, No. 10, 2691–2703, Oct. 2003.
22. Low, Z. N., J. H. Cheong, and C. L. Law, "Low-cost PCB antenna for UWB applications," *IEEE Antennas and Wireless Propagation Letters*, Vol. 4, No. 1, 237–239, 2005.
23. Liang, J., C. C. Chiau, X. Chen, and C. G. Parini, "Study of a printed circular disc monopole antenna for UWB systems," *IEEE Transactions on Antennas and Propagation*, Vol. 53, No. 11, 3500–3504, Nov. 2005.
24. Ojaroudi, N., M. Ojaroudi, and Y. Ebazadeh, "UWB/omni-directional microstrip monopole antenna for microwave imaging applications," *Progress In Electromagnetics Research C*, Vol. 47, 139–146, 2014.
25. Akhoondzadeh-Asl, L., M. Fardis, A. Abolghasemi, and G. R. Dadashzadeh, "Frequency and time domain characteristic of a novel notch frequency UWB antenna," *Progress In Electromagnetics Research*, Vol. 80, 337–348, 2008.
26. Linguraru, M. G., C. Oyarzun Laura, R. Shekhar, S. Wesarg, M. Á. González Ballester, K. Drechsler, Y. Sato, and M. Erdt, *Clinical Image-based Procedures. Translational Research in Medical Imaging*, Vol. 8680, Springer International Publishing, Cham, 2014.
27. Ghanbari, P. and M. Hajj, "Finite element analysis of tissue electropermeability through the application of electric pulses," *J. Bioengineer and Biomedical Sci.*, Vol. 3, No. 120, 2, 2013.
28. Bahramiabarghouei, H., E. Porter, A. Santorelli, B. Gosselin, M. Popovic, and L. A. Rusch, "Flexible 16 antenna array for microwave breast cancer detection," *IEEE Transactions on Biomedical Engineering*, Vol. 62, No. 10, 2516–2525, Oct. 2015.
29. Gabriel, S., R. W. Lau, and C. Gabriel, "The dielectric properties of biological tissues: II. Measurements in the frequency range 10 Hz to 20 GHz," *Physics in Medicine and Biology*, Vol. 41, No. 11, 2251–2269, Nov. 1996.
30. Davarcioglu, B., "The dielectric properties of human body tissues at electromagnetic wave frequencies," *Int. J. Sci. and Adv. Technol*, Vol. 1, No. 5, 12–19, 2011.